

Contents lists available at ScienceDirect

Energy

journal homepage: www.elsevier.com/locate/energy



Experimental electro-hydrodynamic investigation of flag-based energy harvesting in the wake of inverted C-shape cylinder



U. Latif ^{a, b}, E. Uddin ^{a, *}, M.Y. Younis ^c, J. Aslam ^a, Z. Ali ^a, M. Sajid ^a, A. Abdelkefi ^d

- a Department of Mechanical Engineering, School of Mechanical and Manufacturing Engineering, National University of Sciences and Technology, Islamabad,
- ^b Department of Mechanical Engineering and Materials Science, Duke University, Durham, NC, 27708, USA
- ^c Department of Mechanical Engineering, Mirpur University of Sciences and Technology, Mirpur, Pakistan
- d Department of Mechanical and Aerospace Engineering, New Mexico State University, Las Cruces, NM, 88003, USA

ARTICLE INFO

Article history: Received 26 June 2020 Received in revised form 7 October 2020 Accepted 28 October 2020 Available online 30 October 2020

Keywords: Inverted C-shape cylinder Piezoelectric-flag Energy harvesting Shedding frequency PIV

ABSTRACT

Series of water tunnel experiments are performed to study the improvement in energy harvesting by vortex-induced vibrations. Inverted C-shape cylinders with different cut angles are placed in the uniform fluid flow and electrical energy is harvested using the undulating behavior of the piezo-flag in the downstream vortices. Experimental results demonstrate different flapping modes like poorly and optimal coupling with the wake flow. It is also showed that the streamwise gap and flow speed have a significant impact on the amplitude and flapping frequency, which results in the variation of the energy output of piezo-flag. The results indicate that the highest gain in output power is 66% for an inverted Cshape cylinder with a 120° cut angle compared to a circular cylinder performance. For each cylinder and flow velocity, it is also observed that there exists a critical streamwise gap for which vortex shedding does not produce any energy using piezo-flag due to poor coupling with wake flow. The results show that there is no significant difference in the performance of circular and 60° inverted C-shape cylinders regarding energy harvesting. However, changing the shape and cut angle leads to a remarkable increase in the flapping amplitude and its growth rate along with the dominant frequency, Particle Image Velocimetry (PIV) experimentation also endorses the results as wake dynamics is in good agreement with the energy efficiency improvement. Therefore, a 120° cut angle configuration holds a vivid preeminence over a circular cylinder as the kinetic source of a fluid energy harvester. The present study contributes effectively to harvesting energy from impinging vortices by tuning the streamwise gap, flow velocity, and cut angle of the inverted C-shape cylinder.

© 2020 Elsevier Ltd. All rights reserved.

1. Introduction

A huge population of the world is still using conventional energy resources which leads to emissions of greenhouse gases, global deforestation, global warming, and ultimately adverse effects on human health [1]. Clean energy production got attention using renewable sources of energy to reduce dependency on conventional sources. Due to this renewable energy, efficient electronic devices were also made. The vast developments in the field of micro-electromechanical systems (MEMS) and electronic sensor devices considerably reduce the micro-sensor power requirements. These sensors require a few microwatts of energy to operate

properly. Therefore, the harvested electrical energy for these sensors at a small scale using piezoelectric material is sufficient to operate them efficiently like wireless sensor nodes for structural and human health monitoring, cardiac pacemaker, and quartz watch [2–4]. The harvested energy can also be increased easily by using multiple piezoelectric membranes in optimized circuit design [5,6]. It is getting more feasible to integrate the autonomous power sources with such devices instead of the conventional battery packs. This approach would not only be environment friendly but would also reduce operational and maintenance costs [7–11].

One possible source of renewable energy is to extract energy using vortex-induced vibrations (VIV), which is common in nature. Smit and Allen [12] introduced the use of flowing energy by converting it to electrical energy with the help of the piezoelectric membrane. The flexible piezoelectric membrane oscillates like

^{*} Corresponding author.

E-mail address: emaduddin@smme.nust.edu.pk (E. Uddin).

cantilever plates or beams with large flapping amplitude (deformation) and frequency when exposed to wake flow and is advantageous for energy harvesting [13—15]. Wang et al. [16] made a comprehensive review and summarized the various techniques and models of energy harvesting for flow-induced vibrations (FIV). Williamson [17] presented a detailed study about the dynamics of the vortex structure behind a circular bluff body from the creation of shear layers till damping of the vortex. The downstream flexible body can overcome its drag and make efficient use of vortex shedding for passive propulsion/flapping [18]. Parametric studies have been conducted for harvesting energy from vortex-induced vibrations in the water/oceanic environment [19—24].

Various studies are carried out to harvest the energy contained by the vortices shedded by the bluff body. Goushcha et al. [25] examined energy harvesting by placing a cantilever piezoelectric beam in the wakes of a vortex generator and measured the pressure distribution and deformation of the beam due to vortices of different strength by the vortex generator. Shi et al. [26] performed experimentation in a water channel to study the effect of aspect ratio on the performance of energy harvesting and to study the effect on amplitude, lock-in, Reynolds number, and strain distributions. Bluff bodies with different cross-sections like a circular, square, rectangular, triangular prism, pentagon, quasi-trapezoid, and cir-tria prism were used to enhance the performance of energy harvesting, which reported 26.5% and 45.7% increase in efficiency numerically [27,28]. However, such numerical models did not provide a realistic estimation of the harvested power, lacked experimental validation, and were restricted to 2D simulations. Zhang et al. [29] proposed the interference cylinder with different cross-sections to enhance transverse vibration resulting in higher voltage output using the wake galloping phenomenon. A small but continuous amount of energy was harvested by converting flow energy to electrical energy; many studies were conducted to boost its efficiency and analyzing the dynamics of the flag with and without the bluff body.

Several researchers [30,31] used the tandem arrangement to show the interaction behavior, hydrodynamic drafting, constructive and destructive modes, and to improve the efficiency of the energy harvesting system. Shan et al. [32] showed that the output power of 167.8 µW was attained at the water flow velocity of 0.306 m/s and the spacing ratio between two cylinders of 2.5. Similarly, the generation of the peak to peak output voltage of 0.12 V and an instantaneous power output of 0.7 nW was obtained when the pressure of Karman vortex street fluctuates with an amplitude of 0.3 kPa and a frequency of 52 Hz [33]. Zhang et al. [34] studied the effect of resonance on energy harvesting experimentally with peculiar features of Strouhal number, fluctuation in coefficients of lift and drag. The detailed numerical analysis was presented by Song et al. [35] which conforming to their experimental results and witnessed maximum power of 84.49 µW with 60.35 mW/m² energy density at 0.35 m/s velocity with resonance vibration. They recommended a larger diameter of the attached cylinder and lighter weight mass for better performance which showed the pivotal role of the bluff body in improving the efficiency of energy harvesting.

In other kinds of studies, the bluff body was used as a tip mass to instigate the galloping to enhance the capability of energy harvesting along with synchronizing the vortex shedding frequency with the natural frequency of the energy harvester to create resonance transversely [36,37]. Besides, different techniques and configurations had been recommended to improve the performance of these energy harvesters including the modification of the bluff body by converting it to Y-shape, T shape, Arc shape, equilateral prism-shaped and D shape [38–44]. Those previous studies did not

place the piezoelectric flag inside the wake region freely as it was attached to the beam/substrate which was directly connected to the bluff body. Hence, no direct impact of the interaction of shedded vortices or cylinder wakes on the piezoelectric flag was examined. The phenomenon adopted in these studies was galloping or a combination of VIV and galloping which are quite different and represent movement induced excitation (MIE). Whereas the one used in the current study deals with instability induced excitation (IIE) due to wake flow [45]. Although these are different studies with different phenomena but discussed here to highlight the fact that the shape change of the bluff body has a substantial impact and boosts the energy efficiency of energy harvesting systems. Moreover, no study has been conducted for extracting energy from inverted C-shape cylinder by placing a piezoelectric flag in the wake of the bluff body, by changing the streamwise gap distances and flow velocity.

The present study aims to examine the effects of the spacing between the inverted C-shape cylinder and piezo-flag (G_x) , flow velocity (U), and cut angles (α) on the electro-hydrodynamic performance of energy harvesters. The study shows significant benefits of utilizing an inverted C-shape cylinder for improvement in wake dynamics like wake width and formation length, which leads to improvement in the energy harvesting capability of the proposed system as compared to its counterparts. PIV experimentation is carried out to determine how the wake changes and affects the output power as the flag can oscillate with maximum amplitude behind any bluff body equals to its wake width [12]. Therefore, if the wake width increases, the output power will also increase. The circular cylinder is taken as a baseline case as it is used in previous studies for energy harvesting from wake flow [46,47]. However, energy harvesting from VIV using bluff bodies with different crosssections is not yet well understood. The cut angle of the inverted Cshape cylinder is varied from 0°-180°. A range of flow velocities (0.17–0.31 m/s) are studied to observe the cut-in speed, where the proposed system attains efficient performance. Streamwise gaps are also varied between 0.5 and 3.0, which completely covers the entire wake of the cylinder, to find the most appropriate gap for optimal coupling of wake flow with the piezo flag. This considered approach addresses limitations and key challenges from earlier studies and demonstrates a new concept of energy harvesters that could be employed in an estuary/fluctuating conditions.

The experimental setup to study the impact of these parameters is explained in the next section. Section 3 deals with the results and discussion of the effect of the system's key parameters on the efficiency of power generation, and then annotation of the overall behavior of all cylinders is also presented at the end of the results and discussion section. Based on the obtained experimental results, conclusions are drawn and presented in the last section.

2. Experimental setup

Experiments are conducted in the low-speed closed-circuit water channel facility of the Department of Mechanical Engineering, School of Mechanical and Manufacturing Engineering at the National University of Sciences and Technology (NUST) [48]. Channel had a square test section having dimensions (L \times W \times H) $2\times0.4\times0.4$ m. Honeycombs made of aluminum with the hexagon openings and dimensions $1.83\times0.50\times0.025$ m (L \times W \times H) are used to make the flow uniform [Fig. 1(c)]. A variable frequency drive (VFD) motor is used to vary the freestream velocity (U_{∞}) in the range of 0–0.5 m/s with a maximum turbulence intensity of less than 1%. The complete experimental setup along with the schematic is shown in Fig. 1. Enhancement in energy harvesting by the flag is investigated by placing it behind an inverted C-shape

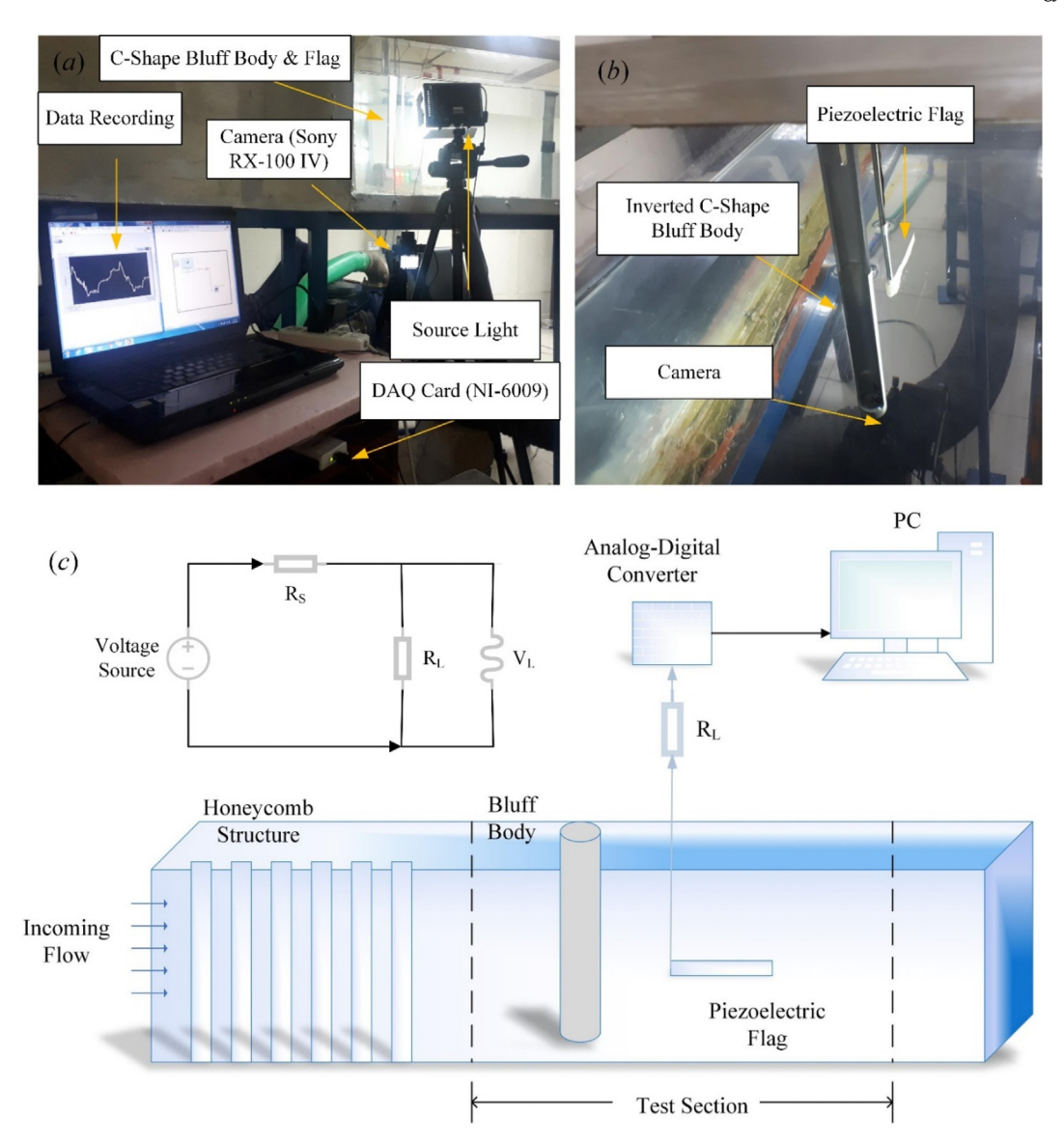


Fig. 1. Experimental setup: (a) complete setup including test section with an inverted C-shape cylinder and piezoelectric flag, a light source for illumination the test section, camera for recording videos, DAQ, and PC for gathering data; (b) internal view of the test section (showing an inverted C-shape cylinder and flexible flag behind it); and (c) schematic of the complete experimental setup.

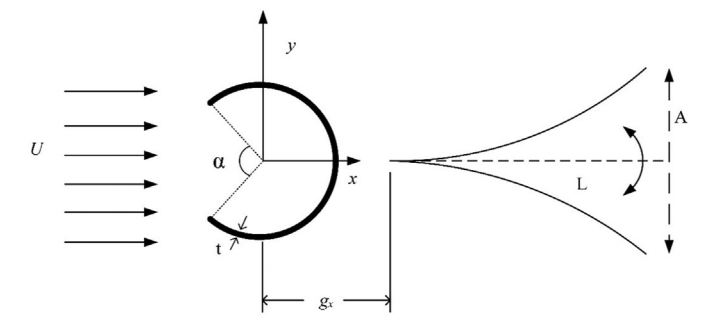


Fig. 2. Schematic of the experimental setup with flag clamped leading end and free trailing end (top view), straight dotted line is the initial position with flag length (L). Flapping in the y-direction with an amplitude (A) taken from peak to peak behind an inverted C-shape cylinder and g_x is the streamwise gap between the cylinder and the piezoelectric flag.

cylinder, as shown in Fig. 2. The maximum blockage ratio observed is 6.25% which is under the acceptable limit as reported by Choi et al. [49]. The cylinder and aluminum rod (used to hold the flag) are mounted tightly with the frame placed on the top of the test section to avoid any vibration or transverse motion. The experimental setup for this study includes a sensor for freestream velocity measurement, a slow-motion camera, a data acquisition system, and a device to measure the voltage across the piezoelectric film made of polyvinylidene fluoride (PVDF) material. The piezo film (54 µm thick) is packed inside thin metalized layers which is used as transportation of charges developed on piezo film/material and further connected to built-in terminals. It is covered with protective layer (transparent thin plastic sheet). Total thickness of piezo membrane is $64 \mu m$ [50]. The amount of energy extraction depends upon the applied force/pressure and strain generated in piezoelectric film. PVDF-DT series piezoelectric film produces more than 10 mV per micro-strain. These films can generate output voltage in the range of 10 mV-100 V depending on circuit impedance and applied force [51].

Table 1Detail of the piezoelectric flag under consideration.

Parameter	Value
Flag total length (mm)	72
Flag active length (mm)	62
Density of flag (Kg/m ³)	1.78
Young's Modulus (10 ⁹ N/m ²)	2-4
Relative permittivity (ϵ/ϵ_0)	12
d_{31} constant (10 ⁻¹² C/N)	23
g_{31} constant (10 ⁻³ Vm/N)	216
k_{31} constant (% at 1 KHz)	12
Capacitance (nF)	1.44
Output voltage (V)	0.01-100
Impedance (M Ω)	1
Operation temperature (°C)	$0 \ to \ +70$

Table 2 Details of the system's parameters.

Parameter	Value
Cylinder diameter (D) (mm)	25
Wall thickness of cylinder (t) (mm)	1.5
C-section cut angle (α)	0°-180°
$G_{x}=g_{x}/D$	0.5-3.0
Blockage ratio	6.25%
Velocity (m/sec)	0.1-0.3
Seed particles for PIV	Hollow glass spheres
Material mean composition (μm)	15
Density (g/cm ³)	1.05
Refractive index	1.5

The flag (PVDF DT2-052 K/L w/rivets, P/N: 2-1003744-0, Measurement Specialties Inc.,) leading edge is fixed with an aluminum rod of diameter, $\Phi = 4$ mm, and the trailing edge is free to move. The flag is of a length of 72 mm with an active length of 62 mm. The width of the flag is 12 mm and the thickness of 64 μ m. The detailed properties of the flag and its material are illustrated in Table 1. The movement of the flag is captured by using a high-speed camera (Sony RX-100 IV). The output wires of the piezoelectric flag are connected with external load resistance R_L (1 M Ω), as shown in Fig. 1(c). The video of each experiment is captured for 120 s at a rate of 50 frames/second for the resolution of 1920 \times 1080 pixels. The piezoelectric film is illuminated using LED lights (Model: Mcopus TTV 204), positioned on each side of the flag for better visualization. The test section is covered with black paper to avoid any background interference in the video. Video data is post-processed using Matlab® to calculate the amplitude and dominant frequency of the flag. Moreover, the data of the energy generated by the PVDF flag is gathered with the data acquisition card (DAQ, National Instruments, NI-USB 6009, multifunction I/O) at 50 Hz for 120 s using LabView®.

Particle image velocimetry is conducted using a MicroVec PIV system consists of a CCD camera (Imprex CLB-B1320M) having a spatial resolution 1280 pixel × 720 pixels, with a maximum sampling frequency of the system is 30fps and 5Watt Diode-pumped solid-state (DPSS) laser with 532 nm wavelength. Tracer particles made of hollow glass and having a density 1.05 g/cm³ are used to identify the flow field in the wake region. To calculate the velocity vectors, the cross-correlation (frame-to-frame) technique is applied [52], using "SM-MICROVEC3, 2D2C PIV/PTV software" (developed

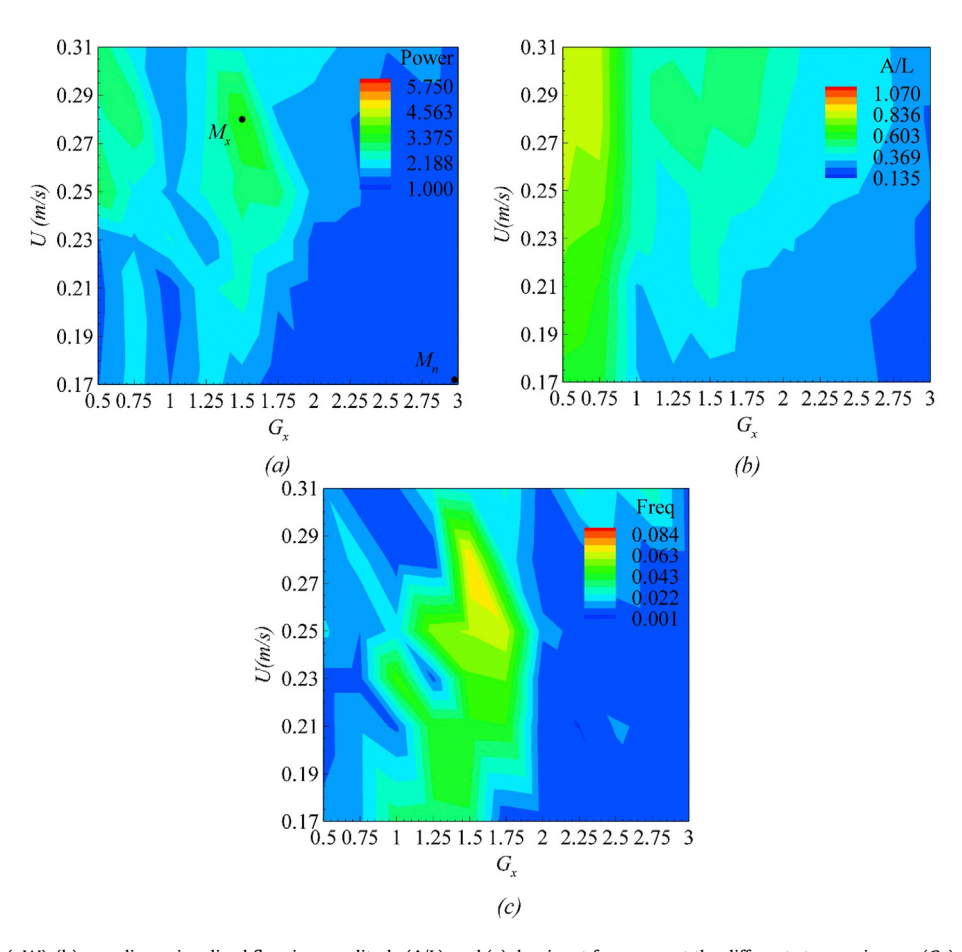


Fig. 3. (a) Harvested power (μ W), (b) non-dimensionalized flapping amplitude (A/L), and (c) dominant frequency at the different streamwise gap (G_x) and flow velocities (U) for a circular cylinder.

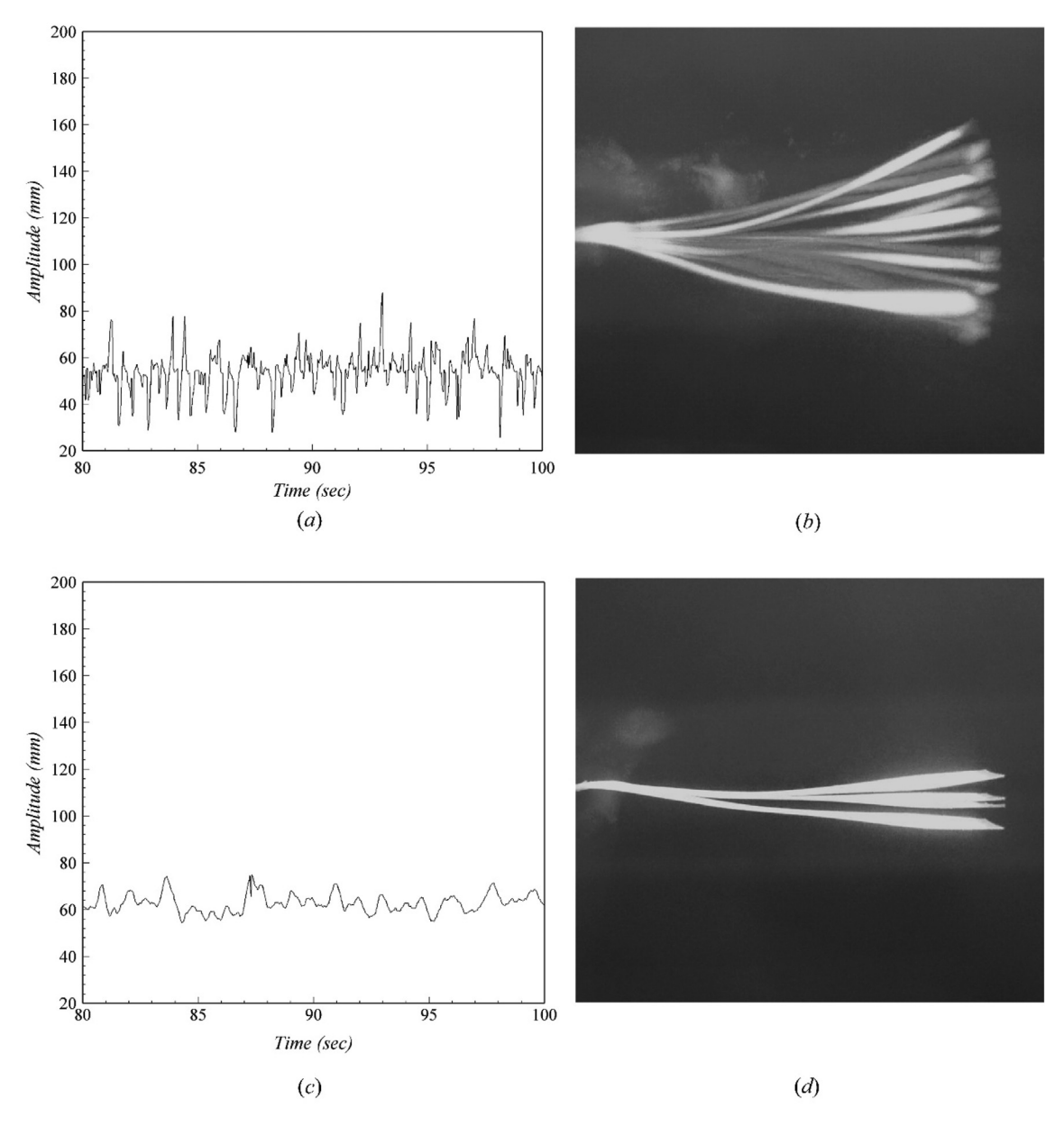


Fig. 4. (a) Variation of the amplitude of flapping with time corresponding to peak power and (b) envelope for peak power point at Mx ($G_x = 1.5$ and U = 0.28 m/s). (c) Variation of the amplitude of flapping with time corresponding to low power and (d) envelope for low power point at Mn ($G_x = 3.0$ and U = 0.17 m/s).

by the World Technology Development Co., Ltd. Beijing) which integrates the PIV, PTV, concentration, and particle size analysis and field analysis module. Details of the parameters used during the experimentations are described in Table 2.

3. Results and discussion

The effects of flow and geometric parameters on the efficiency of the piezoelectric flag using the inverted C-shaped bluff body are deeply investigated in this study. The benchmark circular cylinder is first considered and subsequently change it to an inverted C-shape bluff body angle as shown in Fig. 2. Generally, the experimental results show that the variations in these parameters cause different modes of flapping, and result in improved energy harvesting efficiency.

The piezoelectric flag which is placed in the wake of a cylinder

will inevitably be driven by vortex shedding. So, the flag is subjected to vortices shedded from the upstream cylinder, resulting in deflection of the flag and produces strain in the piezoelectric sheet, and hence electric charge develops in the flag. Alternatively, a combined effect of amplitude and frequency of the flexible flag causes deformation resulting in energy generation due to produced strain. With the beam theory for a given shape, strain energy can be determined in a piezoelectric film. It shows that the energy harvested by the piezoelectric film is a function of film thickness, flapping frequency, the capacitance of the piezoelectric layer, and oscillating amplitude [23]. Michelin [53] and Shoele [54] also showed that the electric voltage generated from the piezoelectric film is directly proportional to the deformation. Using the same principle of energy generation and deformation, the power generated from the piezo-flag and the tail position evolution are experimentally observed. The tail position evolution is post-processed to

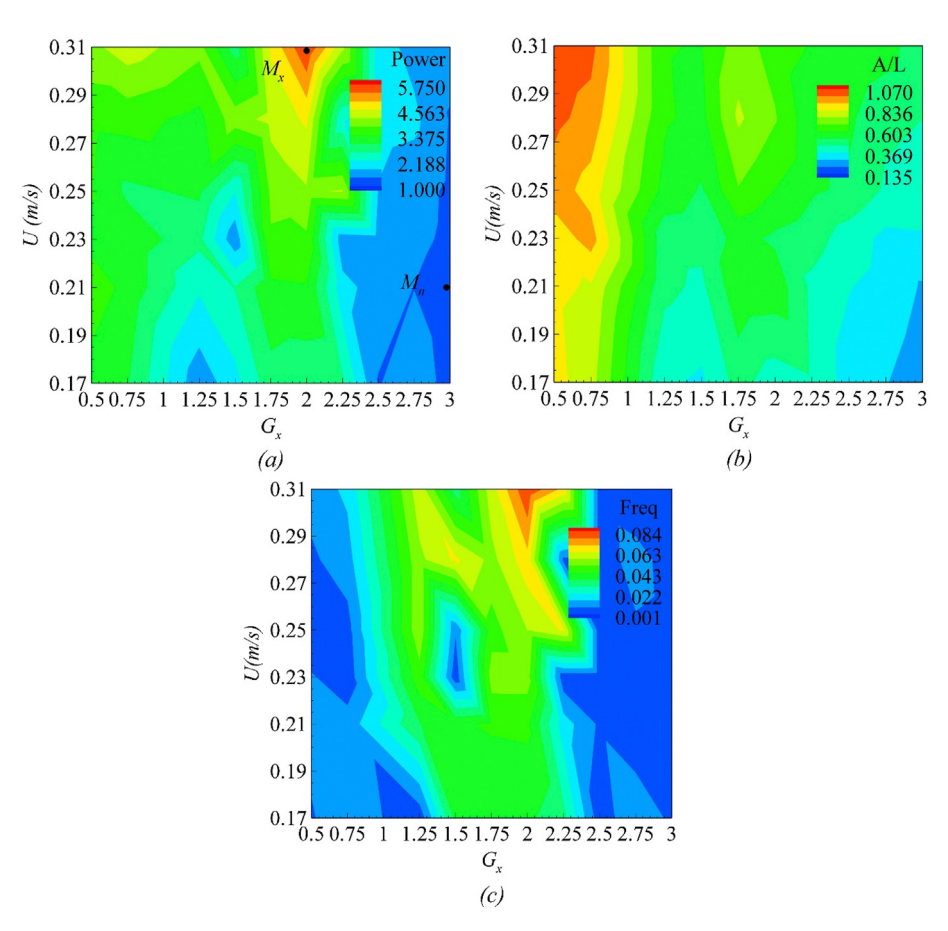


Fig. 5. (a) The harvested power (μW), (b) non-dimensionalized flapping amplitude (A/L), and (c) dominant frequency at the different streamwise gap (G_x) and velocities (U) for 120° inverted C-shape cylinder.

find the dominant frequency and flapping amplitude of the flag. Continuous intermittent and biased flapping modes are observed during experiments. The average harvested power is calculated by using $P = V^2_{rms}/R_L$ where V_{rms} denote root mean square of the generated voltage. By using the maximum power transfer theorem, the value of the external load resistance R_L is set equal to the impedance of the piezoelectric flag to obtain maximum power from the circuit/source [55]. The detailed results of each type of cylinder (cut angle α), distance between the cylindrical bluff body and the piezo-flag (G_X), flow velocity (U) are studied and discussed in the

3.1. Impacts of the inverted C-shape cylinder on the performance of the energy harvester

3.1.1. Circular cylinder

Fig. 3 shows the results of energy harvesting through a piezo-electric flag in the wake of a circular cylindrical bluff body. The plotted curves in Fig. 3(a) presents the effects of the streamwise gap and flow velocity on the output power of the energy harvesting system. It follows from this figure that the highest power output is obtained for the gap distance between $G_X = 0.75-2.0$ and flow velocity between U = 0.23-0.31 m/s. For higher values of the gap distance between the bluff body and the piezo-flag ($G_X > 2$), minimum levels of the harvested power are observed. To investigate this behavior, flapping amplitude and dominant frequency graphs are analyzed, as shown in Fig. 3(b) and (c), respectively. Beyond

 $G_x = 2$, the flapping amplitude and oscillating frequency drop to the lowest value due to which the harvested power is decreased. The highest power obtained for this case is marked at point "Mx" $(G_x = 1.5 \text{ at } U = 0.28 \text{ m/s})$, similarly, the lowest power is marked with "Mn" ($G_x = 3$ at U = 0.17 m/s). It can also be seen from Fig. 3(b) and (c) that there is the highest flapping frequency and amplitude as well, which corresponds to the highest energy generation at the identified point. The tail position evolution and envelope plot for the peak and lowest generation point are shown in Fig. 4(a-d), respectively. The intermittent flapping behavior can be observed in Fig. 4(a) e.g. at T = 85 & 90-91 s. In intermittent flapping, the piezoelectric flag stops flapping for a short time before flapping again. The corresponding graphs further explain the high and low power generation. The flag flaps with an amplitude (A/L) of 0.8 behind a circular bluff body, which is in agreement with the literature results [14].

3.1.2. 120° cut cylinder

For a 120° cut inverted C-shape cylinder, the harvested power, flapping amplitude, and dominant frequency are shown in Fig. 5(a–c), respectively. Inspecting the plots in Fig. 5(a), high energy generation point Mx ($G_x = 2$ at U = 0.31 m/s) is marked. At this point, analysis of the tail position evolution, envelope, and the dominant frequency is carried out, as presented in Fig. 6(a–b). Clearly, a high flapping frequency has taken place. In comparison with all other cut cylinders, the 120° cut cylinder shows the highest amplitude flapping. This is due to the strong coupling between the

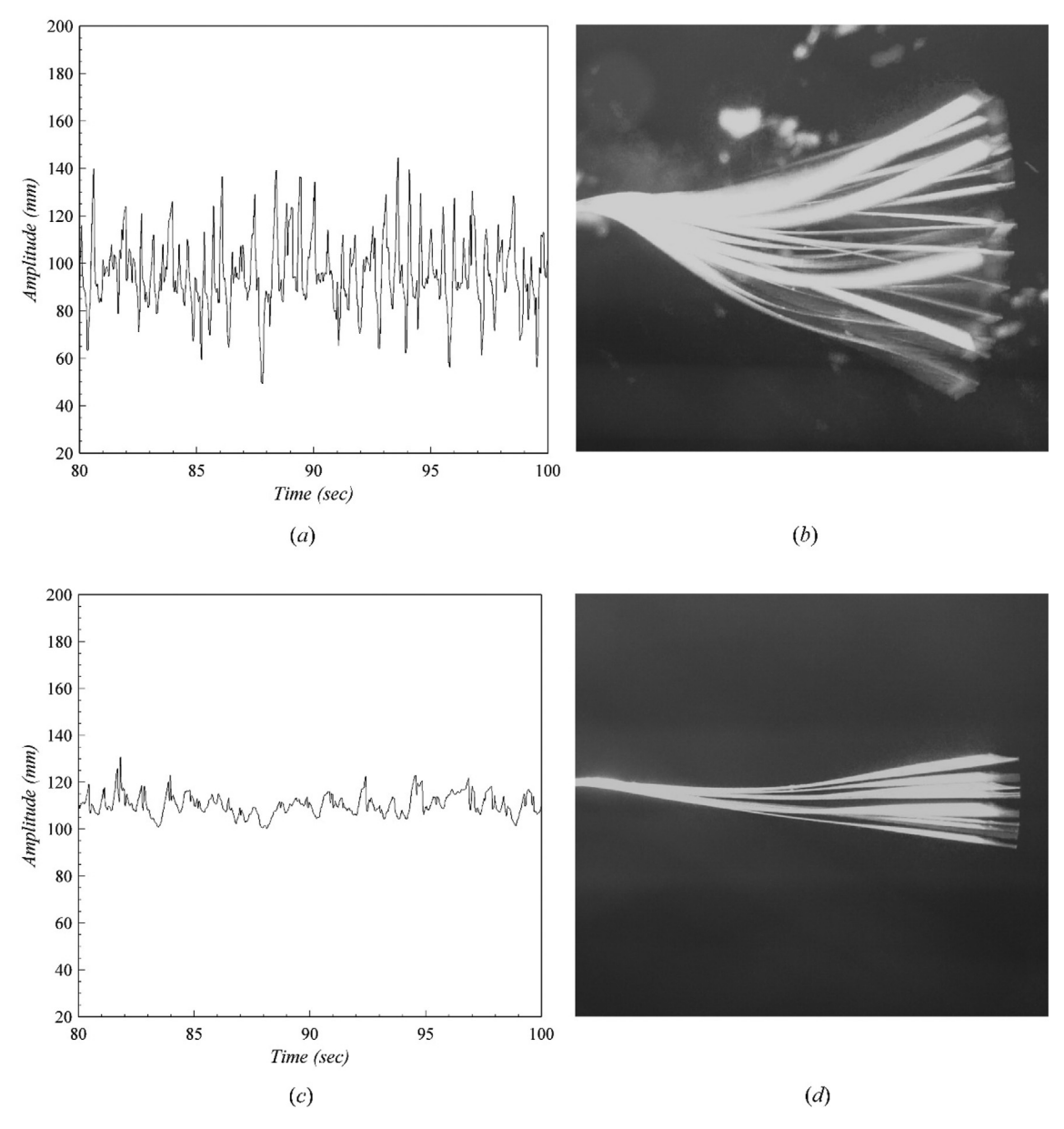


Fig. 6. (a) Variation of the amplitude of flapping with time corresponding to peak power and (b) envelope for peak power point at Mx ($G_x = 2.0$ and U = 0.31 m/s). (c) Variation of the amplitude of flapping with time corresponding to low power and (d) envelope for low power point at Mn ($G_x = 3.0$ and U = 0.21 m/s).

piezoelectric flag and the wake flow (vortex shedding). Bidirectional curvature is obtained with high flapping frequency, which shows the highest energy generation, which conforms to the literature [23] that high curvature and frequency assures high harvested power. However, as indicated in Fig. 5, as the streamwise gap (G_x) between the inverted C-shape cylinder and flag is increased beyond $G_x = 2.5$, a drop in the flapping amplitude, harvested power, and dominant frequency is observed, showing the critical point beyond the stated point. M_n is marked in Fig. 5(a) showing the lowest energy generation point.

To further investigate the performance of piezo-flag energy harvesting systems at the two critical identified points, time histories of the amplitude of flapping and envelope of the deflection of the system are shown in Fig. 6 for the peak power point ($G_x = 2.0$ and U = 0.31 m/s) and low power point ($G_x = 3.0$ and U = 0.17 m/s). By analyzing the plotted curves in Fig. 6(c-d), the undulating flapping of the piezoelectric flag energy harvester is found between

continuous flapping with low amplitude and frequency. In contrary to all other upstream bodies, flapping is observed for all values of G_X and U. Highest values of harvested power, amplitude, and frequency are observed in comparison with other upstream bodies. In comparison with the circular cylinder, the harvested power, flapping amplitude, and frequency for a 120° cut cylinder are increased by 62.29%, 30.25%, and 19.09%, respectively.

3.1.3. 150° cut cylinder

Next, the case of a 150° inverted C-shape cylinder is deeply investigated. The impacts of the gap between the bluff body and energy harvesting system and flow speed are determined as shown in Figs. 7 and 8. Similar experiments are performed compared to the previous two designs. It is found that the two prominent gap regions where continuous energy harvesting occurs *i.e.* $G_X = 0.5-1.0$ and $G_X = 2.25-2.75$. At point " M_X " ($G_X = 2.50$ at U = 0.31 m/s) in Fig. 7(a), a high harvested power value is obtained.

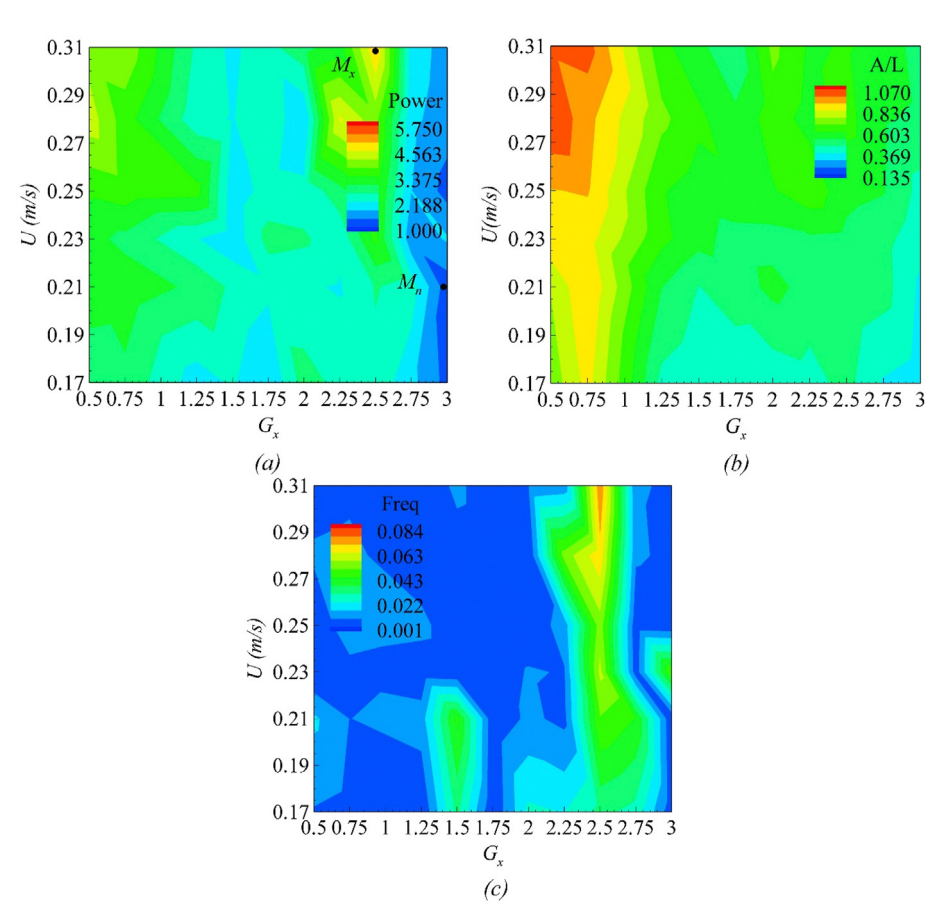


Fig. 7. (a) The harvested power (μ W), (b) non-dimensionalized flapping amplitude (A/L), and (c) dominant frequency at the different streamwise gap (G_x) and velocities (U) for 150° inverted C-shape cylinder.

When the gap between the cylindrical structure and the piezo-flag is in the range between 2.25 and 2.75, the flapping frequency and amplitude are high for higher flow velocities resulting in obtaining higher levels of the harvested energy. Fig. 8(b) shows the high flapping amplitude along with the shape of flapping (a wider region covered by flag while moving across the axis). The power generated by this bluff body (150° cut cylinder) is lower than the 120° cut cylinder scenario even it shows a larger flapping amplitude (1.02 as compared to 0.98). This discrepancy is because of the straight beam like the motion of piezo flag as shown in Fig. 8(b), whereas in the case of cut angle 120°, bending curvature is prominent in Fig. 6(b) which justify higher strain energy for 120° cut angle in comparison to 150°. Fig. 8(a) also explains the flapping behavior of the piezoelectric flag and shows biased flapping behind this cut angle as it can be seen at T = 87-95 s. This result may be explained by the improper synchronization for this cylinder so the flapping frequency has remained low. Similarly, low energy regions are found when $G_X \ge 2.75$ owing to low flapping amplitude and frequency, as can be seen in Fig. 8(c-d) for point M_n ($G_x = 3$ at U = 0.21 m/s) marked in Fig. 7(a). By comparing the results of this inverted Cshape cylinder to a circular cylinder counterpart, an increase is obtained in the harvested power, flapping amplitude, and flapping frequency of 42.53%, 33.59%, and 11.43%, respectively.

3.1.4. 180° cut cylinder

When the flag is placed in the wake of a 180° inverted C-shape cylinder, two regions are found for the high values of harvested power. In both regions, continuous flapping is observed. Fig. 9(a) shows that, for $G_X = 0.5-1.0$, the piezo-flag energy harvester

exhibits flapping with high amplitude with low flapping frequency. For $G_x > 2$, the flapping frequency and amplitude are high due to which high harvested power is produced. For the peak harvested power point Mx ($G_x = 2.75$ at U = 0.31 m/s), the history of the tail position and flag envelope is shown in Fig. 10(a) and (b). The tail history shows continuous flapping for the identified point along with the high value of flapping frequency. For the gap region of $G_x = 1-1.75$, both the flapping amplitude and dominant frequency are low resulting in low power production. As reported by Kim et al. [56], a flapping flag is capable of producing elastic strain energy several times higher than a flag of deformed mode due to the unsteady fluid forces by refining the transformation of fluid kinetic energy to elastic strain. Similarly, point M_n ($G_x = 1.50$ at U = 0.17 m/ s) marked in Fig. 9(a), low harvested power is obtained. The plotted curves in Figs. 9 and 10(c-d) show the poor coupling of the piezoflag energy harvesting system with vortex shedding due to which low flapping amplitude and frequency are observed. In comparison with the circular cylinder experimental results, it is found that there is an increase in the harvested power, flapping amplitude, and flapping frequency with percentages of 53.13%, 31.03%, and 12.47%, respectively.

The optimal and minimum power output points marked in figures of all cylinders are summarized in Table 3. From the above graphs and summary table, it can be observed that the optimal power is obtained at a higher velocity for higher cut angles> 60° , whereas for 60° and circular cylinder, the optimal harvested power is achieved at 0.28 m/s and it decreases with further increase in the flow velocity. A careful analysis of G_X reveals that for higher cut angles, optimal power point shifts from a lower value of G_X to a

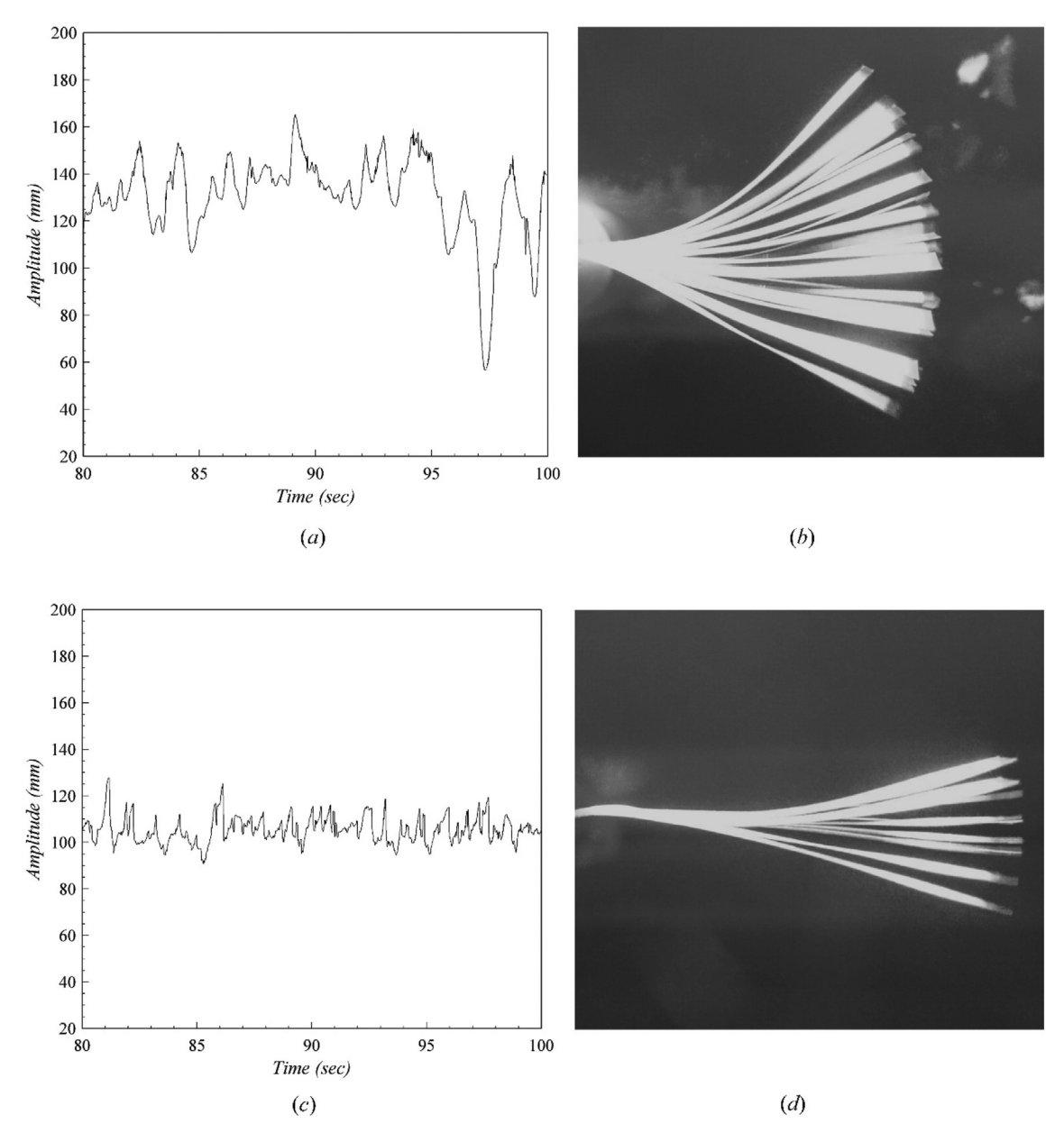


Fig. 8. (a) Variation of the amplitude of flapping with time corresponding to peak power and (b) envelope for peak power point at M_x ($G_x = 2.5$ and U = 0.31 m/s). (c) Variation of the amplitude of flapping with time corresponding to low power and (d) envelope for low power point at M_n ($G_x = 3.0$ and U = 0.21 m/s).

higher value which describes that the expansion in the wake region occurs with the increase of cut angle. Due to this, vortex or free shear layer approaches to the piezoelectric flag after some distance, so optimal coupling with wake flow also occurs at higher G_x and thus optimal energy harvesting performance. Furthermore, a nonlinear trend can be seen in Table 3 for the harvested power which shows the coupling of fluid with the piezoelectric flag is different for different cut angles.

3.2. Impacts of streamwise gap (G_x) on the piezo-flag optimal performance

In previous sections, the influences of the flow velocity and the streamwise gap are discussed for each cut angle. However, for insight evaluation of the energy harvesting efficiency of each bluff body, it is important to analyze the energy harvesting capability of

the bluff body at each streamwise gap individually for the set range of flow velocity, as shown in Fig. 11. When $G_X = 0.5-1.5$, it follows from the plotted curves in Fig. 11(a-d) that all inverted C-shape cylinders including circular (represented with 0) that cut angles show higher energy harvesting efficiency, but the efficiency of energy harvesting of cylinder cut angle of $\alpha=120^\circ$ is maximum. As the value of G_x is raised from 1.5 to 2.0, as indicated in Fig. 11(e-f), the energy harvesting of 120° cut angle cylinder becomes higher especially at U > 0.21 m/s which also shows the critical location of placing piezoelectric flag behind 120° inverted C-shape cylinder for obtaining maximum energy. Concerning the range of gaps higher than 2.25, it is clear that more energy is harvested from higher cut angles ($\alpha > 120^{\circ}$), as presented in Fig. 11(g-i). It can be concluded from these experiments that the increase in streamwise gap especially beyond $G_x = 1.5$, cut angles cylinders show higher efficiency for conversion of fluidic kinetic energy into electrical energy,

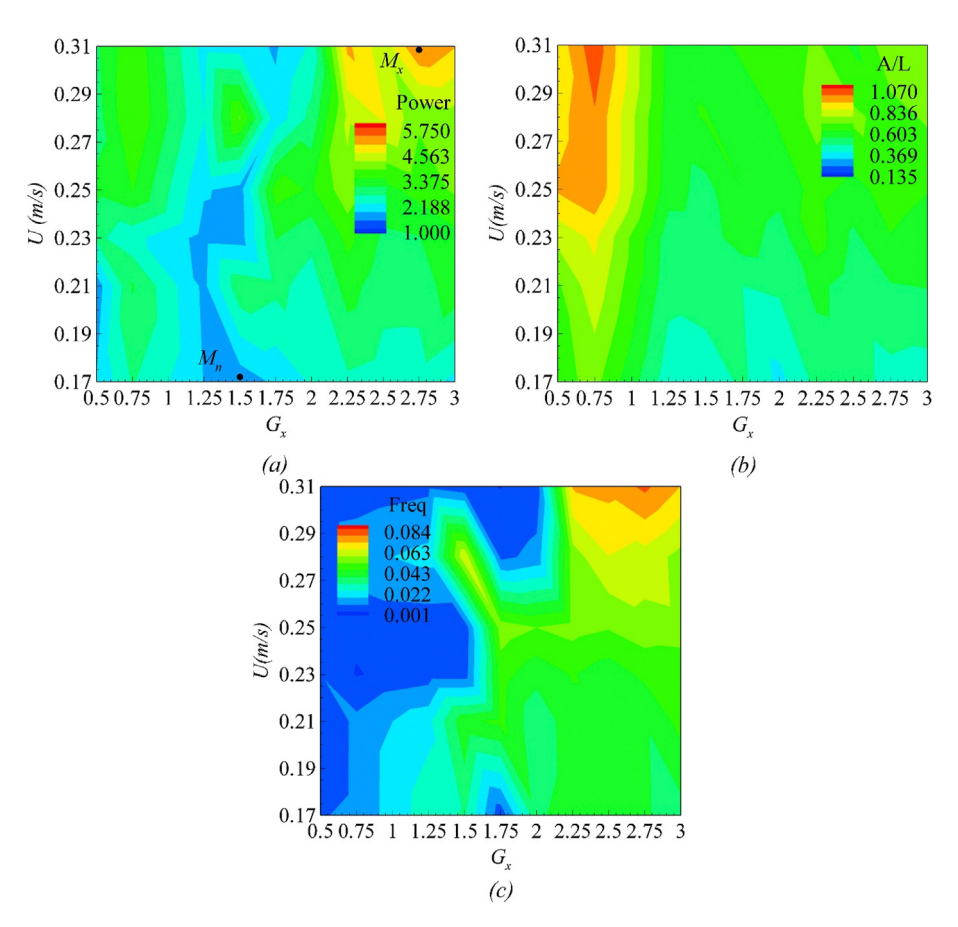


Fig. 9. (a) The harvested power (μ W), (b) non-dimensionalized flapping amplitude (A/L), and (c) dominant frequency at the different streamwise gap (G_x) and velocities (U) for 180° inverted C-shape cylinder.

while the circular cylinder showed minimum energy at such gaps. The detailed analysis of Fig. 11 indicates that every cut angle has a specific gap on which it yields optimal energy harvesting and shows coupling with wake flow.

All the optimal values of the flow velocity and cut angle of the corresponding C-shape cylinder for each streamwise gap are summarized in Table 4. Inspecting the plotted curves in this section and Table 4, it is clear that the dominance of cut angle 120° can be seen for a broader range of $G_{\rm x}$, but for high values of $G_{\rm x}$ (>2.0), the cut angle 120° loses its dominance due to poor coupling of wake flow with the piezoelectric flag. For this range of $G_{\rm x}$, the higher cut angle shows higher energy harvesting capability due to the efficient coupling of wake flow.

3.3. Effects of the flow velocity on the system's optimal response

In addition to the shape of the bluff body and the gap between the energy harvester and the cylinder, the freestream velocity is one of the key parameters on which energy harvesting efficiency depends, as shown in Fig. 12. Indeed, the water speed changes the whole hydrodynamic characteristics of the environment including the Strouhal and Reynolds numbers. Fig. 12(a–f) indicate that energy generation is increased with the increase of freestream velocity almost in a similar pattern. As the flow velocity is increased, the contour shows a systematic increase in color/energy, the green region in Fig. 12(a) turns yellow in Fig. 12(b–d) and then red in Fig. 12(e) and (f). This increase in the flow velocity shows higher energy extraction from vortex-induced vibrations. Because as the core of the vortex gets stronger with the higher velocity, higher

momentum/energy is transferred from vortices to the piezoelectric flag energy harvesting system.

For each flow speed, the optimal configurations for the gap between the inverted C-shape cylinder and the piezo-flag energy harvesting system and the cut angle of the bluff body for each flow velocity used in Fig. 12 are given in Table 5. It follows from Table 5 that for all considered flow velocity values, maximum harvested energy is obtained when the piezoelectric flag is placed behind a cylinder with a cut angle of 120°. Moreover, smaller flow velocities need a smaller gap between the cylinder and the piezoelectric flag. As the flow velocity increases, higher gap distances are required for better coupling between the fluid force and the structure and hence an optimal performance of the energy harvester.

3.4. Annotation of the overall performance of the inverted C-shape cylinders

Harvested power plots give the trend of energy produced concerning the applied fluidic unsteady forces on the flag, which causes deformation and strain change rate in the piezoelectric flag for streamwise gaps (G_x) and velocity ranges. Fig. 13 presents peak net values obtained for each cylinder regarding dominant frequency, flapping amplitude, and harvested power which shows the net output/efficiency of every cylinder with respect to the circular hollow cylinder. Fig. 13 and Table 6 succinctly explain outcomes, after making detailed analysis and comparison with the circular cylinder water tunnel experiments. The performance of the bluff body with cut angles 30° and 60° remain indifferent rather 60° cylinders show a sharp decline in the frequency, as mentioned in

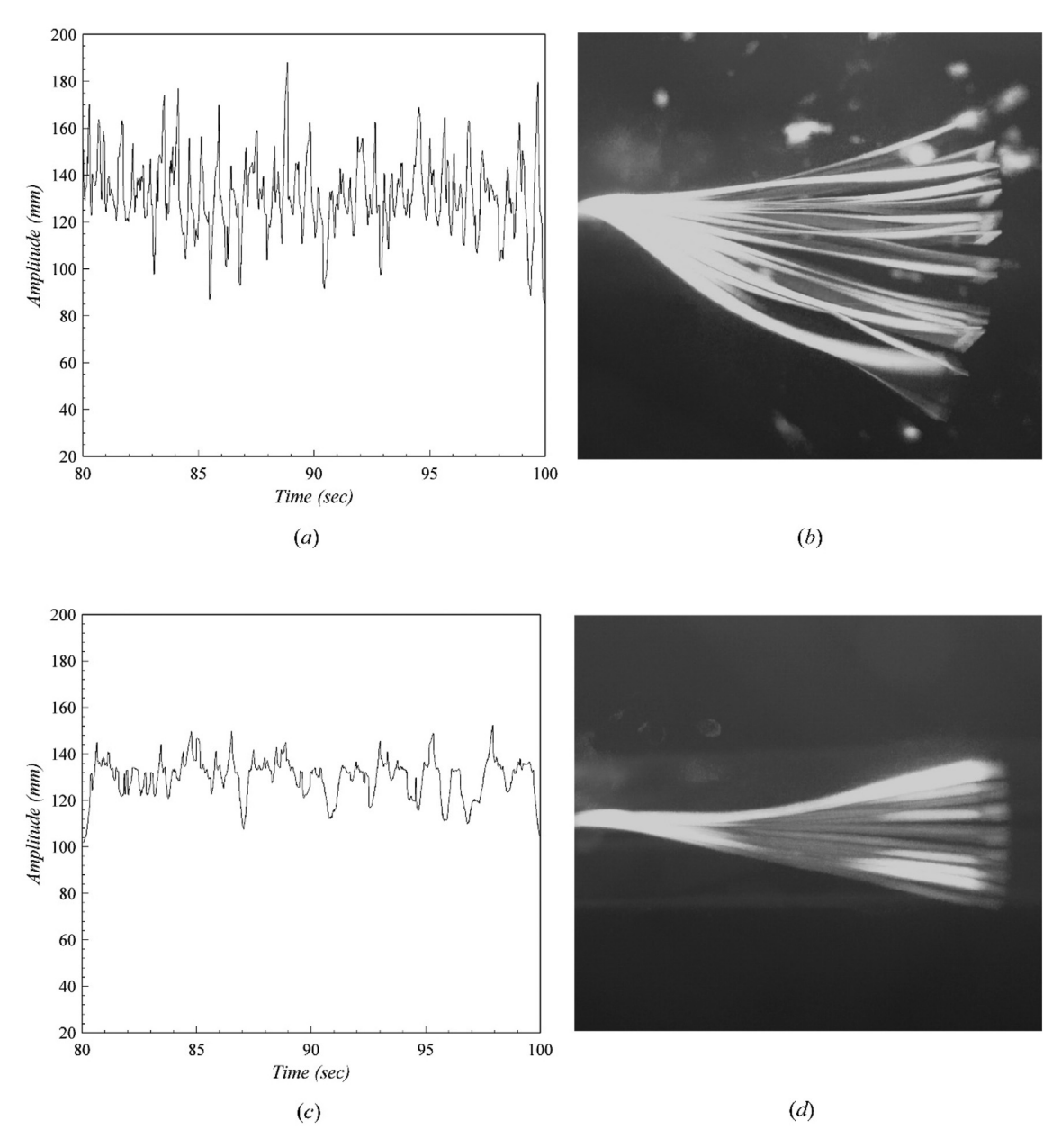


Fig. 10. (a) Variation of the amplitude of flapping with time corresponding to peak power and (b) envelope for peak power point at M_x ($G_x = 2.75$ and U = 0.31 m/s). (c) Variation of the amplitude of flapping with time corresponding to low power and (d) envelope for low power point at M_n ($G_x = 1.50$ and U = 0.17 m/s).

Table 3Summary table for all cylinders with optimal and minimum power output.

Cut angle	Maxima/Minima	U (m/s)	G_{x}	Harvested power (μW)
0	M_{χ}	0.28	1.50	3.460
	M_n	0.17	3.00	1.035
30	M_{χ}	0.31	2.25	3.910
	M_n	0.17	3.00	1.152
60	M_{χ}	0.28	1.25	3.490
	M_n	0.17	3.00	1.047
90	M_{χ}	0.31	0.75	5.210
	M_n	0.17	2.75	1.089
120	M_{χ}	0.31	2.00	5.741
	M_n	0.21	3.00	1.165
150	M_{χ}	0.31	2.50	4.955
	M_n	0.21	3.00	1.168
180	M_{χ}	0.31	2.75	5.369
	M_n	0.21	0.50	1.550

Table 6. By increasing the cut angle from 60° to 180° , higher harvested energy is obtained as compared to the circular cylinder. This explains that there is sufficient energy (proportional to the cube of its velocity) in moving fluid.

An inverted C-shape 120° cylinder is best suited for energy harvesting as it produced energy for a broader range of G_X and U, as shown in Figs. 5, 11 and 12. A detailed analysis of Fig. 13 gives a comprehensive efficiency comparison of all the cylinders, in which cut angle $\alpha=120^\circ$ turned out to be the optimal cut angle for extracting maximum energy from the proposed system. Figures of amplitude plots show detail about the regions of high amplitude *i.e.* $G_X=0.5-2.25$ and $\alpha=90^\circ-180^\circ$. Although for the rest of the regions, the value of the amplitude is lower. Likewise, frequency plots mark regions where the flapping frequency is high and low, high values exists beyond $\alpha\geq90^\circ$. The highest energy generation is attributed to this range, because of the high strain change rate. The

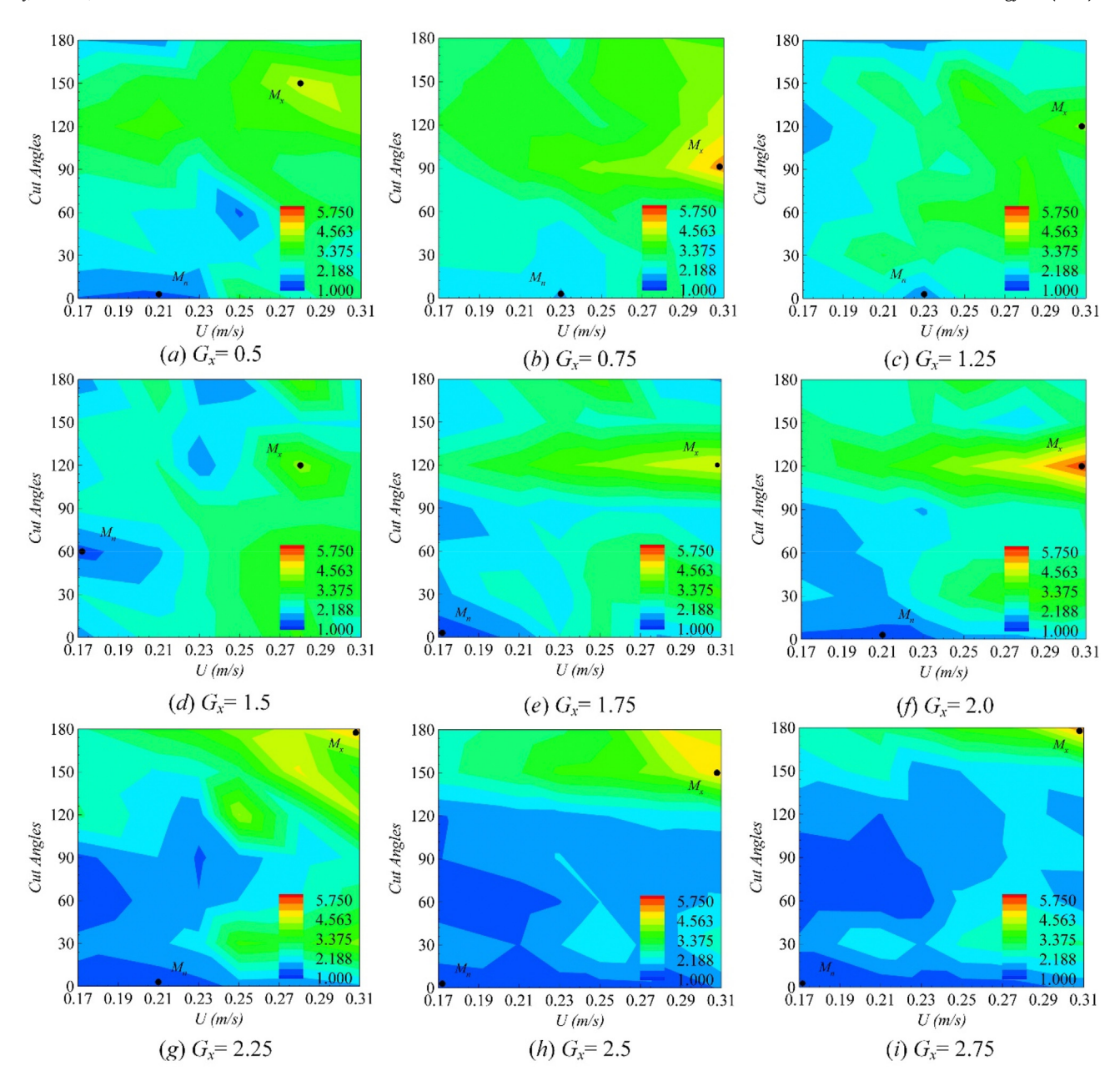


Fig. 11. Harvested power (μ W) at different streamwise gaps (0.5–2.75) for all C-shape cylinders.

Table 4Summary of harvested power for all streamwise gaps.

G_{x}	<i>U</i> (m/s)	Cut angle	Harvested power (μW)
0.50	0.28	150	4.388
0.75	0.31	90	5.210
1.25	0.31	120	3.899
1.50	0.28	120	3.987
1.75	0.31	120	4.626
2.00	0.31	120	5.741
2.25	0.31	180	5.051
2.50	0.31	150	4.955
2.75	0.31	180	5.369
3.00	0.31	180	4.985

interesting thing to note is that the amplitude is very high in this region, while the frequency is comparatively low that shows passive flapping attributed to the hydrodynamic damping due to the viscous fluid. However, it was reported in Ref. [14] that flag flaps with maximum amplitude (*A/L*) of 0.8. However, in this experimental study, it is witnessed an increase of around 34% with the utilization of an inverted C-shape cylinder, which shows a higher percentage gain and promising impact of changing bluff body shape. Likewise, an increase of more than 19% in frequency is observed with the change of bluff body shape. In every inverted C-shape cylinder case, the bi-curvature flapping mode is obtained except 60°. That is the reason due to which the same piezo flag gives 66% higher energy as compared to the circular cylinder.

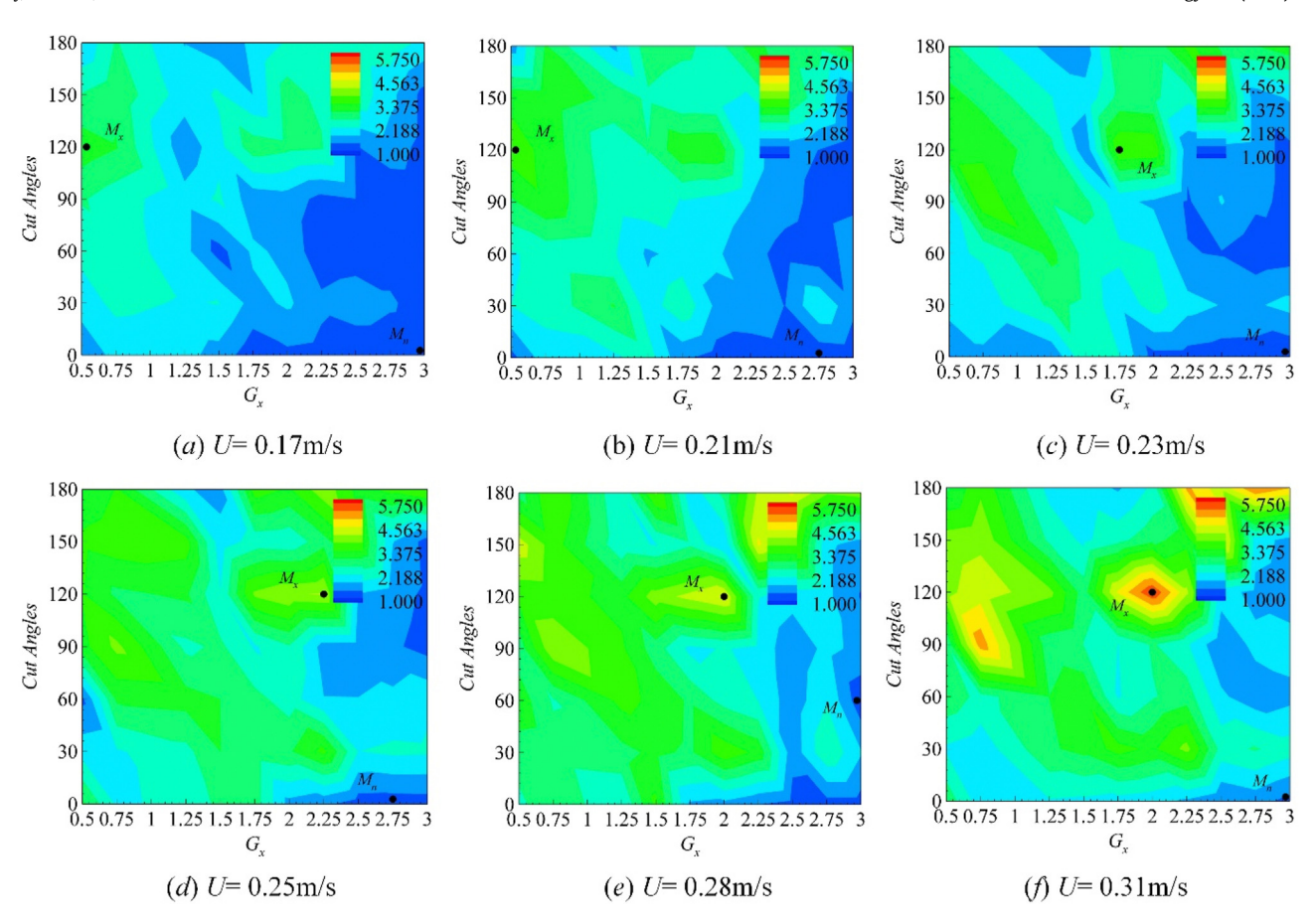


Fig. 12. Harvested power (μ W) at different flow stream velocities (U = 0.17 - 0.31 m/s) for all C-shape cylinders.

Table 5Summary of harvested power for all considered water speed values.

U (m/s)	G_{χ}	Cut angle	Harvested power (μW)
0.17	0.5	120	3.210
0.21	0.5	120	3.592
0.23	1.75	120	3.730
0.25	2.25	120	4.206
0.28	2.0	120	4.626
0.31	2.0	120	5.741

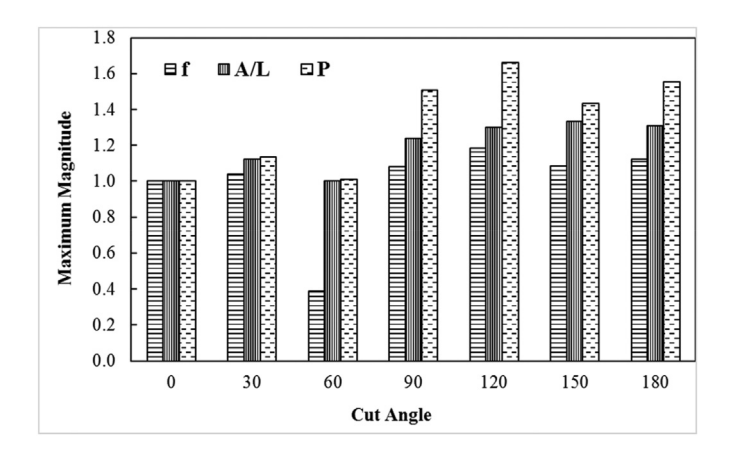


Fig. 13. Peak values obtained for each cylinder regarding dominant frequency (f), flapping amplitude (A/L), and harvested power (P) which shows net output/efficiency of every cylinder (values of dominant frequency (f), flapping amplitude (A/L) and output power (P) are normalized with the circular cylinder value).

3.5. PIV results and system's hydrodynamic characteristics

To have insight information on the energy harvesting and why the different cylinders show different energy harvesting performances, the time-averaged wake of cylinders using particle image velocimetry (PIV) is studied. Time-averaged vorticity $(\overrightarrow{\omega})$ with over-laid mean streamlines for three cylinders are presented in Fig. 14. The particle image velocimetry field of view covering approximately 4.5d in the flow direction and $\pm 1.15d$ in the transverse direction. The field of view is found sufficient to study the time average wake characteristics. The detailed output/performance of each bluff body used is tabulated above, three peak cases selected based on their dissimilar behavior, and PIV experimentation is carried out for getting the clear understanding of the fluidstructure and energy/momentum present in it as these vortical structures drive the piezo flag in the wake region. Flow past a cylinder causes the separated shear layer instability and roll up which in turn results in alternate vortex shedding/Karman Vortex Street in the wake, which contains vortices of opposite rotation (clockwise and anticlockwise direction). The kinetic energy and angular momentum present in it causes energy transfer to the piezoelectric flag energy harvester by producing strain in it with the known phenomenon of fluid-structure interaction. The fluidstructure forming behind circular, 60°, and 120° inverted C-shape cylinders is shown in Fig. 14(a-c) where the piezoelectric flag energy harvesting system is placed. Whereas, flow past the piezoelectric flag is shown in Fig. 14 (a'-c'). These are the average images formed from the 1000 instantaneous data files.

Fig. 14 shows vorticity images with stream tracers behind three

 Table 6

 Percentage increase in output of inverted C-shape cylinders in comparison with a circular cylinder.

C-shape cylinder cut angle	<i>U</i> (m/s)	G_{x}	Normalized frequency	Normalized amplitude (A/L)	Normalized harvested Power
30	0.31	2.25	4.37	12.11	13.02
60	0.28	1.25	61	0.03	0.88
90	0.31	0.75	8.53	23.83	50.60
120	0.31	2.00	19.09	30.25	65.93
150	0.31	2.50	11.43	33.59	43.22
180	0.31	2.75	12.47	31.03	55.19

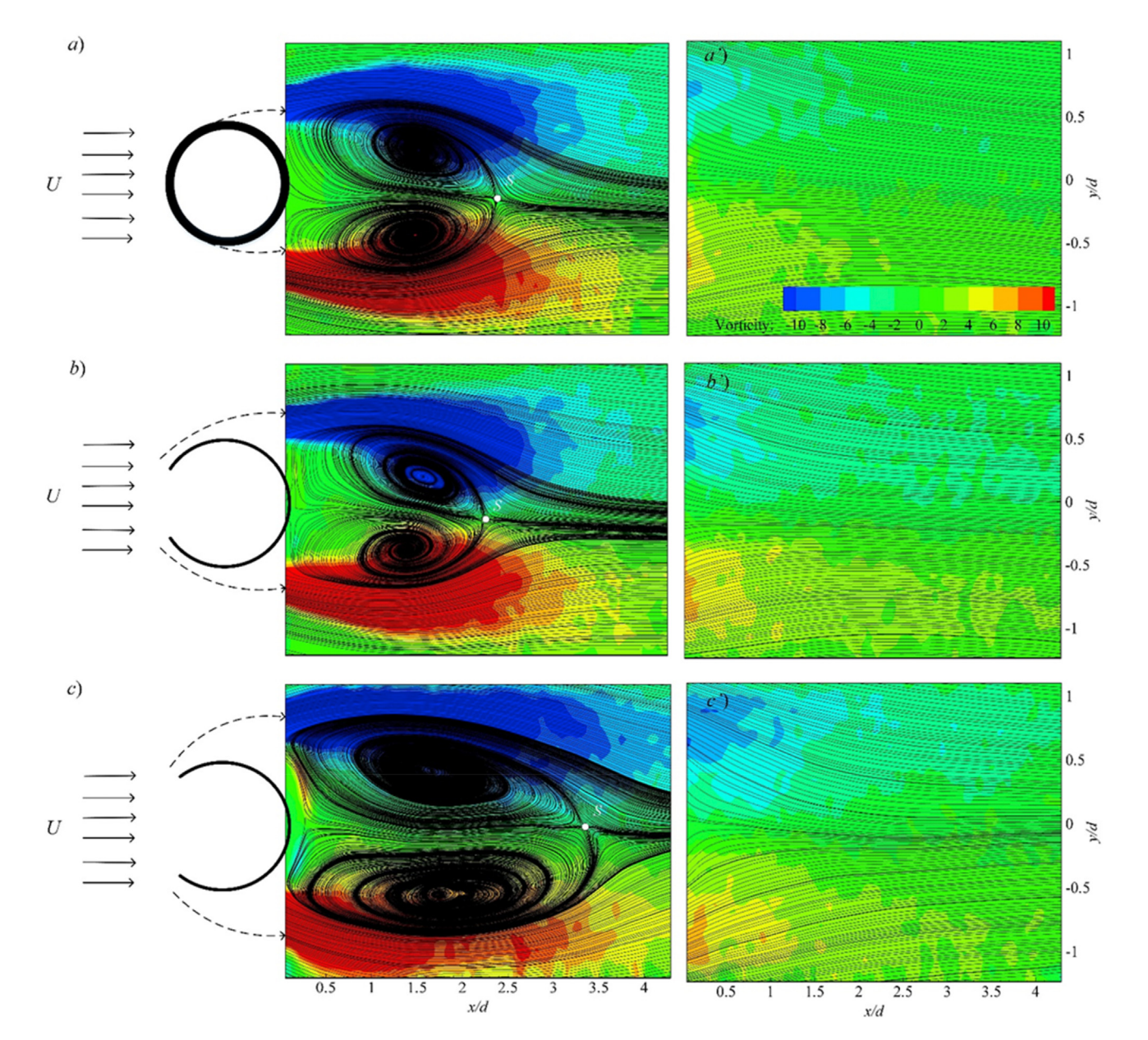


Fig. 14. Formation of the coherent wake behind cylinders without flag and their corresponding flow field (after passing a piezoelectric flag). The plot is drawn by time-averaging for 1000 images.

different bluff bodies without flag and after interacting with the flag for peak energy harvesting point " M_{χ} " of the respective cylinder. Although, the vortex structure behind the cylinder is coherent but strongly turbulent and three-dimensional as well. The piezoelectric flag energy harvesting system in the wake of the bluff body undergoes largely forced oscillations and the averaged vortical

structure, of 1000 images, which interacts with the flag, is highlighted with vorticity contours. The vortical structure formed behind each bluff body is different from one another in every aspect. Although the flow visualizations in Fig. 14(a–c) show an averaged structure without a piezoelectric flag, the overall topologies of the two flows (with and without flag) must be different, as

the flexible flag acts as a streamline to prevent communication between the separating shear layers. The analysis of Fig. 14(a) and (b) reveals that the vortex length behind the circular cylinder is larger as compared to the 60° cut cylinder, which unfolds the reason behind the low dominant frequency of the later one. But, the width of both almost the same which verifies the same flapping amplitude (A/L) as narrated in Table 6.

The interesting thing is that the highest energy for a circular cylinder is obtained when the piezoelectric flag was fixed at $G_x = 1.5$ and the vortex core is also found at the same location, likewise the flag head was fixed at $G_x = 1.25$ for 60° cut angle and the vortex core is at the same location. Similarly, the vortex core for a 120° cut angle is found almost at the same location where it is found the maximum energy output from the piezoelectric flag behind the cylinder. It is evident from the literature that the maximum strength of the vortex exists in the core due to the highest circulation at this point [57]. So, to extract maximum possible energy from the vortex, the piezoelectric flag must be placed at a location where the vortex core approaches its head, and then the traveling vortex will certainly transfer its kinetic energy to flag in terms of mechanical energy in the form of strain. Further analysis and comparison of Fig. 14(c) with Fig. 14(a) and (b) unveils the reason behind the high energy generation when the flag was placed behind a 120° cut cylinder. As it is clear from Fig. 14(c) that the conjectured vortices have higher strength and size in every aspect. Consequently, maximum flow/mechanical energy transfer to the piezoelectric flag resulting in higher electrical energy generation. So, it is clear that the higher the force, the higher would be displacement in terms of deformation of the piezoelectric flag. which have a direct impact on energy generation, resulting in higher harvested energy as the impingement is higher for stronger vortices.

4. Conclusions

The energy harvesting enhancement from the piezoelectric flag excited by impinging vortices produced by an inverted C-shape bluff body has been investigated and discussed. Though the circular cylinder gives consistent power in the range $G_x = 0.5 - 2.0$ beyond U = 0.23 m/s, but 120° C-shape inverted cylinder showed remarkable enhancement in energy harvesting for a broader range of $G_x = 0.5-2.75$ at all velocities with high amplitude (A/L) and frequency (*f*). The low onset flow speed (for $\alpha = 120^{\circ}$) was observed for self-sustained flapping and higher power generation which persist for broader range $G_x = 0.5 - 2.75$, which makes it feasible for implementation in the real environment as air never flows at the same/high speed. One of the outcomes of the study is that the wake dynamics changes including wake width and formation length with cut angles that lead to change in the streamwise gap and velocity for optimal synchronization for every cylinder. Therefore, a 120° inverted C-shape cylinder provided a 33.54% higher flapping amplitude due to its wider wake along with flapping frequency, which are key factors for energy harvesting and cause higher strain in the piezo film. PIV experimentation revealed that optimal best energy results are obtained behind the bluff body when the head of the piezoelectric flag is fixed at a location where time-averaged vortex core exits. Experiments clearly showed that energy harvesting increases with increasing the distance between the C-shape cylinder and flag till $G_x = 2.25$, higher values were obtained at $G_X = 1.25 - 2.25$ for all velocities, U = 0.17 - 0.31 m/s, with $\alpha = 120^{\circ}$ as compared to the circular cylinder. Hence, the stated configuration with $\alpha = 120^{\circ}$ devised a noteworthy advantage over a circular cylinder as a vibration source of a water-energy harvester and the generated power progressively increase with the angle, gap, and speed for a critical range. The harvested power can be used for

powering microelectromechanical sensors installed in remote areas like structural health monitoring by replacing chemical batteries and trickle charge small batteries.

Credit author statement

U. Latif: Conceptualization, Writing- Original draft preparation, Experimentations, Investigation, Visualization; E. Uddin: Supervision, Funding acquisition; M. Y. Younis: Investigation, Visualization; J. Aslam: Writing- Reviewing and Editing, Experimentations; Z. Ali: Validation, Writing- Reviewing and Editing; M. Sajid: Writing-Reviewing and Editing; A. Abdelkefi: Writing- Reviewing and Editing, Investigation.

Declaration of competing interest

The authors declare that they have no known competing financial interests or personal relationships that could have appeared to influence the work reported in this paper.

Acknowledgement

This research was supported by higher education commission of Pakistan grant NRPU 20-4794

References

- Karim ME, Munir AB, Karim MA, Muhammad-Sukki F, Abu-Bakar SH, Sellami N, et al. Energy revolution for our common future: an evaluation of the emerging international renewable energy law. Energies 2018;11. https:// doi.org/10.3390/en11071769.
- [2] Usman M, Hanif A, Kim IH, Jung HJ. Experimental validation of a novel piezoelectric energy harvesting system employing wake galloping phenomenon for a broad wind spectrum. Energy 2018;153:882–9. https://doi.org/ 10.1016/j.energy.2018.04.109.
- [3] Sultana A, Alam MM, Middya TR, Mandal D. A pyroelectric generator as a self-powered temperature sensor for sustainable thermal energy harvesting from waste heat and human body heat. Appl Energy 2018;221:299–307. https://doi.org/10.1016/j.apenergy.2018.04.003.
- [4] Vullers RJM, van Schaijk R, Doms I, Van Hoof C, Mertens R. Micropower energy harvesting. Solid State Electron 2009;53:684–93. https://doi.org/10.1016/ j.sse.2008.12.011.
- [5] Lin HC, Wu PH, Lien IC, Shu YC. Analysis of an array of piezoelectric energy harvesters connected in series. Smart Mater Struct 2013;22. https://doi.org/ 10.1088/0964-1726/22/9/094026.
- [6] Moon JW, Jung HJ, Baek KH, Song D, Kim S Bin, Kim JH, et al. Optimal design and application of a piezoelectric energy harvesting system using multiple piezoelectric modules. J Electroceram 2014;32:396–403. https://doi.org/ 10.1007/s10832-014-9934-0.
- [7] Ottman GK, Hofmann HF, Bhatt AC, Lesieutre GA. Adaptive piezoelectric energy harvesting circuit for wireless remote power supply. IEEE Trans Power Electron 2002;17:669–76. https://doi.org/10.1109/TPEL.2002.802194.
- [8] Priya S. Advances in energy harvesting using low profile piezoelectric transducers. J Electroceram 2007;19:165–82. https://doi.org/10.1007/s10832-007-9043-4.
- [9] Mitcheson PD, Yeatman EM, Rao GK, Holmes AS, Green TC. Energy harvesting from human and machine motion for wireless electronic devices. Proc IEEE 2008;96:1457–86. https://doi.org/10.1109/IPROC.2008.927494.
- [10] Sudevalayam S, Kulkarni P. Energy harvesting sensor nodes: survey and implications. IEEE Commun Surv Tutorials 2011;13:443–61. https://doi.org/10.1109/SURV.2011.060710.00094.
- [11] Song GJ, Cho JY, Kim KB, Ahn JH, Song Y, Hwang W, et al. Development of a pavement block piezoelectric energy harvester for self-powered walkway applications. Appl Energy 2019;256:113916. https://doi.org/10.1016/ j.apenergy.2019.113916.
- [12] Allen JJ, Smits AJ. Energy harvesting EEL. J Fluid Struct 2001;15:629–40. https://doi.org/10.1006/jfls.2000.0355.
- [13] Kim H, Kang S, Kim D. Dynamics of a flag behind a bluff body. J Fluid Struct 2017;71:1–14. https://doi.org/10.1016/j.jfluidstructs.2017.03.001.
- [14] Orrego S, Shoele K, Ruas A, Doran K, Caggiano B, Mittal R, et al. Harvesting ambient wind energy with an inverted piezoelectric flag. Appl Energy 2017;194:212–22. https://doi.org/10.1016/j.apenergy.2017.03.016.
- [15] Silva-Leon J, Cioncolini A, Nabawy MRA, Revell A, Kennaugh A. Simultaneous wind and solar energy harvesting with inverted flags. Appl Energy 2019;239: 846–58. https://doi.org/10.1016/j.apenergy.2019.01.246.
- [16] Wang J, Geng L, Ding L, Zhu H, Yurchenko D. The state-of-the-art review on

- energy harvesting from fl ow-induced vibrations. Appl Energy 2020;267: 114902. https://doi.org/10.1016/j.apenergy.2020.114902.
- [17] Williamson c. Vortex dynamics in the cylinder wake. Annu Rev Fluid Mech 1996;28:477–539. https://doi.org/10.1146/annurev.fluid.28.1.477.
- [18] Triantafyllou MS, Liao JC, Lauder GV, Beal DN, Hover FS. Passive propulsion in vortex wakes. J Fluid Mech 2006;549:385. https://doi.org/10.1017/ s0022112005007925.
- [19] Abdelkefi A. Aeroelastic energy harvesting: A review. International Journal of Engineering Science 2016:100:112—35.
- [20] Tanaka Y, Oko T, Mutsuda H, Patel R, McWilliam S, Popov AA. An experimental study of wave power generation using a flexible piezoelectric device. J Ocean Wind Energy 2015;2:28—36.
- [21] Pan F, Xu Z, Jin L, Pan P, Gao X. Designed simulation and experiment of a piezoelectric energy harvesting system based on vortex-induced vibration. IEEE Trans Ind Appl 2017;53:3890-7. https://doi.org/10.1109/ TIA.2017.2687401.
- [22] Shi S, New TH, Liu Y. Flapping dynamics of a low aspect-ratio energy-har-vesting membrane immersed in a square cylinder wake. Exp Therm Fluid Sci 2013;46:151–61. https://doi.org/10.1016/j.expthermflusci.2012.12.007.
- [23] Techet AH, Allen JJ, Smits AJ. Piezoelectric eels for energy harvesting in the ocean. Proc Twelfth Int Polar Eng Conf 2002;3:713–8.
 [24] Taylor GW, Burns JR, Kammann SM, Powers WB, Welsh TR. The energy harvesting in the ocean.
- [24] Taylor GW, Burns JR, Kammann SM, Powers WB, Welsh TR. The energy harvesting Eel: a small subsurface ocean/river power generator. IEEE J Ocean Eng 2001;26:539–47. https://doi.org/10.1109/48.972090.
- [25] Goushcha O, Elvin N, Andreopoulos Y. Interactions of vortices with a flexible beam with applications in fluidic energy harvesting. Appl Phys Lett 2014;104: 1–6. https://doi.org/10.1063/1.4861927.
- [26] Shi S, New TH, Liu Y. Effects of aspect-ratio on the flapping behaviour of energy-harvesting membrane. Exp Therm Fluid Sci 2014;52:339—46. https:// doi.org/10.1016/j.expthermflusci.2013.09.014.
- [27] Zhang B, Song B, Mao Z, Tian W, Li B. Numerical investigation on VIV energy harvesting of bluff bodies with different cross sections in tandem arrangement. Energy 2017;133:723–36. https://doi.org/10.1016/ i.energy.2017.05.051.
- [28] Ding L, Zhang L, Wu C, Mao X, Jiang D. Flow induced motion and energy harvesting of bluff bodies with different cross sections. Energy Convers Manag 2015;91:416–26. https://doi.org/10.1016/j.enconman.2014.12.039.
- [29] Zhang LB, Dai HL, Abdelkefi A, Wang L. Experimental investigation of aerodynamic energy harvester with different interference cylinder cross-sections. Energy 2019;167:970–81. https://doi.org/10.1016/j.energy.2018.11.059.
- [30] Kim S, Huang WX, Sung HJ. Constructive and destructive interaction modes between two tandem flexible flags in viscous flow. J Fluid Mech 2010;661: 511–21. https://doi.org/10.1017/S0022112010003514.
- [31] Huang H, Wei H, Lu XY. Coupling performance of tandem flexible inverted flags in a uniform flow. J Fluid Mech 2018;837:461–76. https://doi.org/ 10.1017/ifm.2017.875.
- [32] Shan X, Song R, Fan M, Xie T. Energy-harvesting performances of two tandem piezoelectric energy harvesters with cylinders in water. Appl Sci 2016;6:230. https://doi.org/10.3390/app6080230.
- [33] Wang D-A, Pham H-T, Chao C-W, Chen JM. A piezoelectric energy harvester based on pressure fluctuations in Karman vortex street. 8–13 May, 2011, Linköping, Sweden Proc World Renew Energy Congr – Sweden 2011;57: 1456–63. https://doi.org/10.3384/ecp110571456.
- [34] Zhang LB, Dai HL, Abdelkefi A, Wang L. Improving the performance of aeroelastic energy harvesters by an interference cylinder. Appl Phys Lett 2017;111:073904. https://doi.org/10.1063/1.4999765.
- [35] Song R, Shan X, Lv F, Xie T. A study of vortex-induced energy harvesting from water using PZT piezoelectric cantilever with cylindrical extension. Ceram Int

- 2015;41:S768. https://doi.org/10.1016/j.ceramint.2015.03.262. 73.
- [36] Dai H, Abdelkefi A, Wang L. Theoretical modeling and nonlinear analysis of piezoelectric energy harvesting from vortex-induced vibrations. J Intell Mater Syst Struct 2014;25:1861–74. https://doi.org/10.1177/1045389X14538329.
- [37] Mehmood A, Abdelkefi A, Hajj M, Nayfeh A, Akhtar I, Nuhait A. Piezoelectric energy harvesting from vortex-induced vibrations of circular cylinder. Journal of Sound and Vibration 2013;332;4656–67.
- [38] Liu FR, Zou HX, Zhang WM, Peng ZK, Meng G. Y-type three-blade bluff body for wind energy harvesting. Appl Phys Lett 2018;112:1–6. https://doi.org/ 10.1063/1.5029415.
- [39] Kwon SD. A T-shaped piezoelectric cantilever for fluid energy harvesting. Appl Phys Lett 2010;97:164102. https://doi.org/10.1063/1.3503609.
- [40] Zhang X, Yang W, Zuo M, Tan H, Fan H, Mao Q, et al. An arc-shaped piezoelectric bistable vibration energy harvester: modeling and experiments. Sensors 2018;18:4472. https://doi.org/10.3390/s18124472.
- [41] Zhang J, Liu F, Lian J, Yan X, Ren Q. Flow induced vibration and energy extraction of an equilateral triangle prism at different system damping ratios. Energies 2016;9:938. https://doi.org/10.3390/en9110938.
- [42] Abdelkefi A, Yan Z, Hajj M. Performance analysis of galloping-based piezoaeroelastic energy harvesters with different cross-section geometries. Journal of Intelligent Material Systems and Structures 2014;25:246–56.
- [43] Hu G, Tse KT, Wei M, Naseer R, Abdelkefi A, Kwok KCS. Experimental investigation on the efficiency of circular cylinder-based wind energy harvester with different rod-shaped attachments. Appl Energy 2018;226:682–9. https://doi.org/10.1016/j.apenergy.2018.06.056.
- [44] Abdelkefi A, Hajj M, Nayfeh A. Piezoelectric energy harvesting from transverse galloping of bluff bodies. Smart Materials and Structures 2012;22:015014.
- [45] Vxeplwwhg D, Dqg WR, Ri H, Dqg Q, Ri Q, Wkh DQG, et al. On the Interaction between vortex-induced vibrations and galloping in rectangular cylinders of low side ratio. 2016.
- [46] Latif U, Uddin E, Abdullah C, Ali Z, Sajid M, Akhtar K, et al. Experimental investigation of energy harvesting behind a bluff body. J Renew Sustain Energy 2020;12:033301. https://doi.org/10.1063/1.5144347.
- [47] AkaydIn HD, Elvin N, Andreopoulos Y. Wake of a cylinder: a paradigm for energy harvesting with piezoelectric materials. Exp Fluid 2010;49:291–304. https://doi.org/10.1007/s00348-010-0871-7.
- [48] Saeed M, Uddin E, Mubashar A, Zahir SU, Zaidi AA. Design and development of low-speed water tunnel. In: Proc 2018 15th int bhurban conf appl sci technol IBCAST 2018 2018; 2018. https://doi.org/10.1109/IBCAST.2018.8312288.
- [49] Choi CK, Kwon DK. Wind tunnel blockage effects on aerodynamic behavior of bluff body. Wind Struct An Int J 1998;1:351–64. https://doi.org/10.12989/ was.1998.1.4.351.
- [50] Solutions TES. DT series elements with lead attachment. Measurement 2006: 4297. 4297.
- [51] Specialties M. Piezo film sensors technical manual. Measurement 2006;57.
- [52] Pte M. Micro Vec Pte. Ltd n.d.
- [53] Michelin S, Doaré O. Energy harvesting efficiency of piezoelectric flags in axial flows. J Fluid Mech 2013;714:489–504. https://doi.org/10.1017/jfm.2012.494.
- [54] Shoele K, Mittal R. Energy harvesting by flow-induced flutter in a simple model of an inverted piezoelectric flag. J Fluid Mech 2016;790:582–606. https://doi.org/10.1017/jfm.2016.40.
- [55] Poole C, Darwazeh I. Introduction. 2016. https://doi.org/10.1016/b978-0-12-407823-9.00001-9.
- [56] Kim D, Cossé J, Huertas Cerdeira C, Gharib M. Flapping dynamics of an inverted flag. J Fluid Mech 2013;736:1–12. https://doi.org/10.1017/ jfm.2013.555.
- [57] Currie IG. Fundamental mechanics of fluids. third ed. New York: CRC Press; 2016